Iranian Journal of Science and Technology, Transactions of Civil Engineering (2024) 48:3103–3117
https://doi.org/10.1007/s40996-024-01520-8

RESEARCH PAPER

The Effect of CFRP Application on the Strength and Dynamic Characteristic of Unreinforced Masonry Wall

Adamou Marou Seyni Samberou[1] · Şevket Ateş[1] · Barbaros Atmaca[1]

Received: 5 August 2022 / Accepted: 19 June 2024 / Published online: 7 July 2024

Abstract

This paper presents the results of experimental and analytical investigations of an unreinforced masonry wall (URM) exposed to continuous tensile-compressive cyclic loading. For the experimental investigation, a sample masonry wall (SMW) was designed inside a rectangular steel frame carried by pinned supports and built over a distance of 1200 mm in length by 1500 mm in height. The SMW was made of bricks whose dimensions were 285 mm × 185 mm × 130 mm. Under the influence of cyclic loading, damages appeared as diagonal or scattered cracks. The SMW was retrofitted by using carbon fiber-reinforced polymer (CFRP). An epoxy resin-based product and layers of CFRP were placed on the damaged SMW according to the crack patterns to acquire better recovery, effective strengthening, and enhanced performance. The retrofitted SMW underwent the same cyclic loading to obtain the effects of CFRP on the load–displacement capacity of the damaged masonry wall. Furthermore, an operational modal analysis test was conducted over SMW (the undamaged, the undamaged and retrofitted with CFRP) to determine their real dynamic characteristics. For analytical investigations, finite element analysis (FEA) was implemented in ABAQUS software with a simplified micro-modeling approach and damages were considered only in terms of displacement in this work. Nonlinear cyclic analysis was performed to obtain crack patterns and displacements. To determine modal parameters such as mode shapes and frequencies, modal analysis was also conducted. The obtained results such as displacements, damage patterns and modal parameters from analytical investigations were compared with experimental investigations. In the comparison of analytical and experimental studies, the results showed that the dynamic characteristics such as mode shapes and natural frequencies of SMW were changed. The use of CFRP increased up to 36% of the frequencies of the damaged sample wall. Furthermore, the shear strength capacity of SMW retrofitted by CFRP was significantly increase.

Keywords Simplified micro-modelling · Unreinforced masonry wall · Nonlinear analysis · Dynamic characteristics · Cyclic loading · CFRP · Epoxy-resin

1 Introduction

The materials used in unreinforced masonry walls (URM) are usually blocking or stones, combined with mortar, and provide an anisotropic and nonlinear character to the masonry wall. These varieties in mechanical properties make the modeling task more complicated especially when it comes to certain categories of modelling. There are mainly two types of modeling in the literature such as macro-modeling and micro-modeling.

The macro modeling strategies in masonry walls consist of developing a heterogeneous structure composed of units and mortar through Finite Element (FE) software as a single homogeneous model. This approach adjusts both materials and their properties to obtain a continuum element (Lourenço 1997). In macro modeling, the Distinct Element Method (DEM) can be used to determine out-of-plane shear and flexural failure modes and at the same time simulate in-plane damage (Malomo and Dejong 2021). Other previous studies used out-of-plane loads on macro modeling procedures through the Method of Cells with the application

✉ Barbaros Atmaca
atmaca@ktu.edu.tr

Adamou Marou Seyni Samberou
adamou.samberou@gmail.com

Şevket Ateş
sates@ktu.edu.tr

[1] Department of Civil Engineering, Karadeniz Technical University, Trabzon, Turkey

of the kinematic theorem for limit analysis. These studies obtained the upper bounds to the macroscopic strength domain of the wall in the space of the macroscopic bending and twisting moments (Milani and Taliercio 2016). The macro modeling strategies are convenient for large structures since computational efforts are not excessive; however, they offer less accurate results. The micro-modeling is subdivided into two groups according to their approach: the detailed and the simplified micro-modeling. The detailed approach represents every aspect of the bound elements such as the units, mortar, and interfaces. It is considered a discontinuum element in which joints can act as planes of weakness. It is a technically complex process because it involves a lot of input values and consumes a lot of time. This discontinuum property of the micro-modelling has been used in stone masonry walls by (Pulatsu et al. (2021) to simulate the cracking and shear failure modes within the stone units in the spatial and non-spatial stochastic domain. In other aspects, Sarhosis and Lemos (2018) presented the analysis of masonry couplets and prisms in detailed micro-modeling. Their studies have shown that the mechanical behavior of masonry depends on the properties of irregular particles and the contacts between the brick and the mortar in which the failure occurs. Greco et al. (2020) identified a failure at the brick/mortar interface level, and it was attained by using a cohesive-frictional interface approach for joints and simulating multiple micro-crack inception and propagation. Whereas the mortar is absent the simplified micro-modeling expanded unit bounds are used between them through interfaces. The modeling and analysis process in the case of simplified micro-modeling demands less computer processor and time than detailed micro-modeling.

There are numerous studies about URM according to modeling types given previously. Page (1978) was the first to propose a simplified micro model by assuming the masonry units as a continuum, in which the thickness of the interfaces is neglected. Based on the same concept, Lotfi and Shing (1994) studied the nonlinearity at joints under compressive and tensile shear forces that generated the vertical crack initiation. However, Lourenço and Rots (1997) presented the performance of the interface elastoplastic constitutive model for the determination of URM behavior. They showed the performance of the mentioned model by the result of different masonry shear wall sample. Oliveira and Lourenço (2004) showed failure surfaces on interface elements by using plasticity theory with the unloading/reloading behavior. Chaimoon and Attard (2007) improved the Ferris and Tin-Loi (2001) concrete fracture approach, which consists of splitting into triangular FE units and simulating fracture. However, Oschsendorf and Lorenzis (2008) performed studies over rectangular masonry buttresses under an arch or arch load by applying concentrated load with discrete analysis and considering the structure as a continuum model. Abdulla et al. (2017) proposed an extended finite element method (XFEM) for a three-dimensional nonlinear masonry under cyclic loads based on determining the elastic and plastic behavior of joints, without defining an initial crack propagation. Also, other researchers presented results based on their investigations on the effects of cyclic forces in-plane and out-of-plane. This is the case of Aref and Dolatshahi (2013) who simulated a 3-D model with ABAQUS which is subject to an in-plane and out-of-plane cyclic loading through a subroutine to analyze both linear and nonlinear performance.

Moreover, polymer composite materials are increasingly used to improve and rehabilitate the resistance capacities of existing structures (Ali et al. 2021; Smits 2016; Russell et al. 2017; Uyttersprot et al. 2021). The fibers of these materials are often derived from carbon, basalt, aramid, and glass. Overall, the term most used to refer to these fibers is FRP (Fiber Reinforced Polymer) and can be named in a specific way according to the materials that mainly compose them, such as: AFRP (Aramid Fiber Reinforced Polymer), BFRP (Basalt Fiber Reinforced Polymer), GFRP (Glass Fiber Reinforced Polymer), and CFRP (Carbon Fiber Reinforced Polymer). FRP reinforcement for masonry structures offers several advantages over traditional reinforcement methods, such as steel reinforcement bars (rebars) or wire mesh. Here are some ways in which FRP reinforcement can be advantageous such as corrosion resistance, lightweight, high strength-to-weight ratio, non-conductive, ease of installation, durability, design flexibility, and improved structural performance. Their field of application is varied and has been the subject of several studies depending on the structure to be strengthened. Hamzeh et al. (2020) applied (GFRP) bars on reinforced masonry shear walls enhancing their performance. Stratford et al. (2004) tested reinforced walls with FRP layers under a load of a monotonic shear load. At the end of their study, they obtain an increase in shear strength capacity.Marcari et al. (2007) examined the in-plane behavior of masonry walls with different FRP strengthening patterns under monotonic shear-compression loading in a quasi-static test. They concluded that the shear strength of the wall is significantly increased by using FRP. Santa-Maria and Alcaino (2011) used FRP to repair four masonry walls that were damaged. Then two configurations of externally bonded carbon fiber strips were applied and tested under cyclic shear loading up to failure. They discovered that shear damage was achieved when the force exerted resulted in maximum deformation, and FRP-repaired walls may recover the initial lateral stiffness depending on the retrofitting pattern. Bernat-Masó and Gil (2019) focused on the role of fiber reinforcement in mode shapes of masonry walls. Fifteen walls were built with five sorts of carbon-FRP schemes. A comparison of analytical and experimental frequencies was made, which demonstrated that the rise in

the amount of the FRP increased the frequency variation and reduced the damping ratio.

As seen in the literature, some studies have focused on the effects of cyclic forces in-plane and out-of-plane behavior of models using macro and micro-modeling procedures. Some of them have investigated the performance of CFRP when used for repairing the damaged masonry wall and a limited number of studies have presented the role of fiber reinforcement on mode shapes of masonry walls. However, this study is intended to cover all of the above-mentioned issues. This paper aims to show the performance of CRFP on the strength and dynamic characteristic of a masonry wall. A sample masonry wall (SMW) was designed and exposed to continuous tensile-compressive cyclic loading to determine the crack pattern for the experimental investigation. The damaged SMW was retrofitted by CFRP. The retrofitted SMW underwent the same cyclic loading to obtain the effects of CFRP on the load–displacement capacity of the damaged masonry wall. Additionally, an operational modal analysis test was conducted over three SMWs (undamaged, damaged, and retrofitted with CFRP) to determine their real dynamic characteristics. For analytical investigations, finite element analysis (FEA) was implemented in ABAQUS software with a simplified micro-modeling approach for determining damages. Modal analysis was also conducted to determine modal parameters such as mode shapes and frequencies. The obtained results such as displacements, damage patterns, and modal parameters from analytical investigations were compared with experimental investigations. The rest of the manuscript is arranged as follows. Section 2 presents the description of the test setup and instrumentation. Section 3 describes the analytical approach for crack simulation and the result of SMW exposed to cycling load according to experimental and analytical investigation. The definition of modal analysis and operational modal analysis is given in Sect. 4. The comparison of operational and FE modal analysis is given in Sect. 5. The conclusions are presented in Sect. 6.

2 Test Setup and Instrumentation

In the literature, different test setups, especially such as direct and indirect load paths, have been used for shear walls. In this study, a new experimental setup which consists of two vertical steel bars with pin supports, on which two other horizontal bars are placed, was designed to provide equal end rotations (Sesli and Husem 2021). Although base pin assemblies were fixed on the floor, top pin assemblies were fixed on a stiff loading beam. If the lateral loads of the wall piers vary due to the tributary inertial mass, large axial forces may develop in the beam, but the floor slabs and in-plane stiffness of the coupled shear walls may produce axial restraint. The axial restraint was compensated with the stiff loading beam. In the designed test setup, lateral loads were transferred to the loading beam connected to the wall piers with pin assemblies using a 100-kN actuator. Linear Potentiometric Displacement Transducers (LPDTs) were used to measure the displacements. An LPDT was placed horizontally in the direction of movement of the loading beam to measure the lateral displacement of the loading beam. The dimensions of the wall were 1200 mm long and 1500 mm high. The general view of the experimental setup is given in Fig. 1. The steel material of the setup is the standard wide flanged. The wide-flanged beam due to its distinctive shape, is very effective in carrying loads. It can bear excessive amounts of pressure and ensure structural stability. The material properties of the wide flange are given in Table 1. To create the sample of masonry wall (SMW), the type of bricks that meets Turkish TS EN 771-1 standard (En 2011) was used. The dimensions of the bricks were 285 mm×185 mm×130 mm. These bricks are vertically perforated as shown in Fig. 2. The drawn and experimental model of SMW is shown in Fig. 3.

3 Analytical Approach for Cracks Simulation

For FEA, a series of blocks and steel frames were designed, assigning them elastic material properties including Concrete Damage Plasticity (CDP) properties for the bricks as shown in Table 2. CDP allowed to simulate nonlinear response for quasi-brittle material and to anticipate the masonry behavior (Bolhassani et al. 2015). The density of bricks was taken according to the value offered by the manufacturer, Young's Modulus and Poisson ratio were taken from the previous study (Lourenço and Rots 1997). In tensile behavior parameters, G_f^I represents the fracture energy that consents to the post-cracking response in the simulation. The G_f^I value for mortar and concrete is around 0.1N/mm (ABAQUS ABAQUS online documentation (2014); Restuccia et al. (2020) and (Khatieb 2016)).

3.1 Simplified Micro-Modeling Wall Concept

Cohesive element COH3D8 (an 8-node Three-Dimensional Cohesive element) found in ABAQUS (ABAQUS online documentation (2014)) was selected insofar as it offers adhesive properties that can replace the complexities observed in interfaces at the detailed micro-modeling (Fig. 4). Under the influence of the applied load, the two surfaces of the cohesive elements separate from each other and the relationship between traction load and separation follows the defined constitutive law. The simplified micro-modeling involves expanded units, with no mortar but with an interface having similar properties existing between mortar and units (Fig. 5).

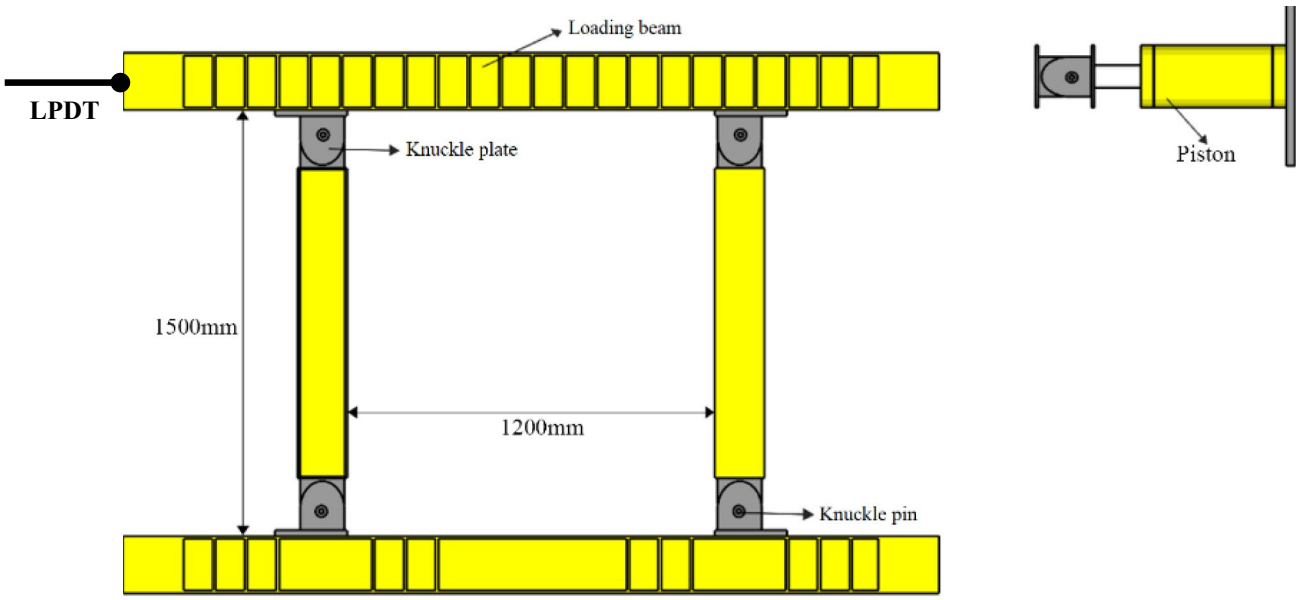

Fig. 1 Frame design

Table 1 Wide-flanged beam properties

Steel		
Density d_1 (t/mm^3)	Young's modulus E_1 (MPa)	Poisson's ratio υ
7.7E-09	2E+05	0.30

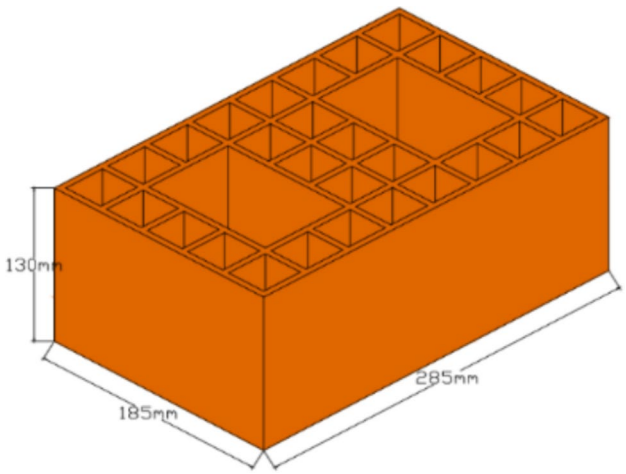

Fig. 2 Vertical hole brick

However, other material considerations also play a preponderant function through the interfaces. That is, the stiffnesses (K_{nn}, $K_{ss,}$ and K_{tt}) support the elastic response across joints. As it is a case of simplified micro-modeling which is used in this article, the interfaces are formed by a new layer that takes into account both the properties of the mortar and the brick. On the other hand, at the level of the contacts, a new adhesive layer is generated which involves friction between different elements at the level of the cohesive interface zones. The ABAQUS program presents values for the contacts between elements. The formulations (1) and (2) were taken from the [9 and 14].

$$K_{nn} = \frac{E_u E_m}{h_m(E_u - E_m)} \tag{1}$$

$$K_{ss} = K_{tt} = \frac{G_u G_m}{h_m(G_u - G_m)} \tag{2}$$

where E_u and E_m are Young's moduli for unit and mortar (MPa), h_m is thickness of joint (mm), K_{nn} is stiffness of masonry joints in the normal direction (N/mm); K_{ss} is stiffness of masonry joints in the first shear direction (N/mm); K_{tt} is stiffness of masonry joints in the second shear direction (N/mm); G_m is the shear modulus of mortar (MPa); G_u is the shear modulus of units (MPa). It should be noted that the coefficient of friction must be considered since it acts on the sliding of different elements. The properties of the perforated brick interface element are given in Table 3.

Simplified micro-modeling was made possible because of using the theory of the discrete elements. The discrete element theory assumes that the elements that make up a system are deformable or changeable under the action of dynamic forces. The Discrete Element Method (DEM), also called the differential element method, is part of a family of numerical methods that allow calculating the motion and effect of large numbers of small particles.

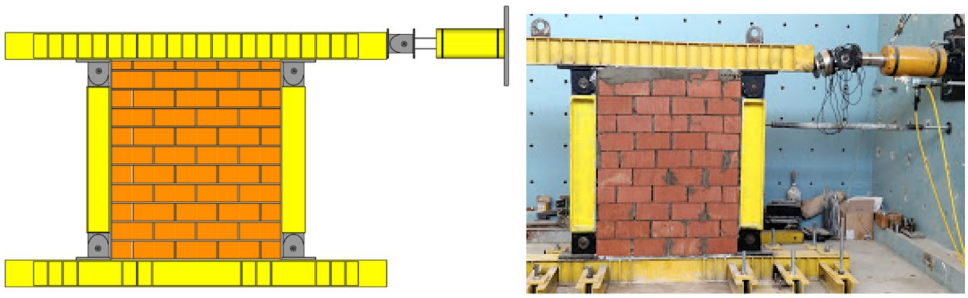

(a) Drawn model (b) Experimental model

Fig. 3 The view of SMW **a** drawn model **b** experimental model

Table 2 Elastic properties of bricks

Vertical hole brick							
Density d_2 (t/mm^3)	Young's modulus E_2 (MPa)	Poisson's ratio υ	CDP (concrete damage plasticity)				
			Dilation angle ψ (°)	Eccentricity	f_{b0}/f_{c0}	K	Viscosity
1.6E-09	16,700	0.20	30	0.1	1.16	0.67	0.002

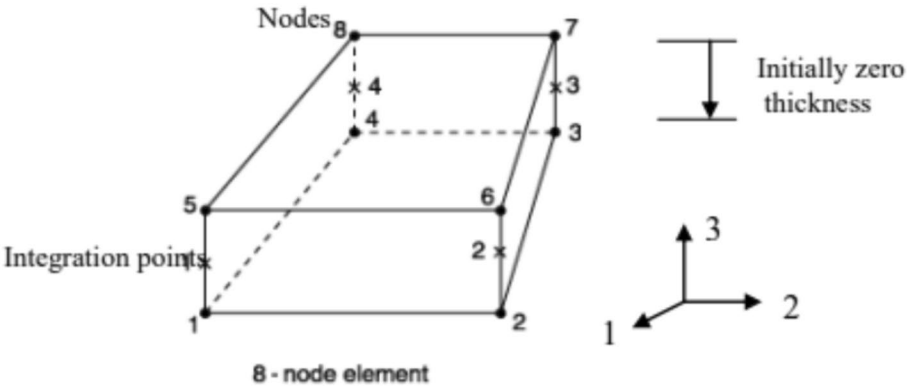

Fig. 4 The COH3D8 cohesive element

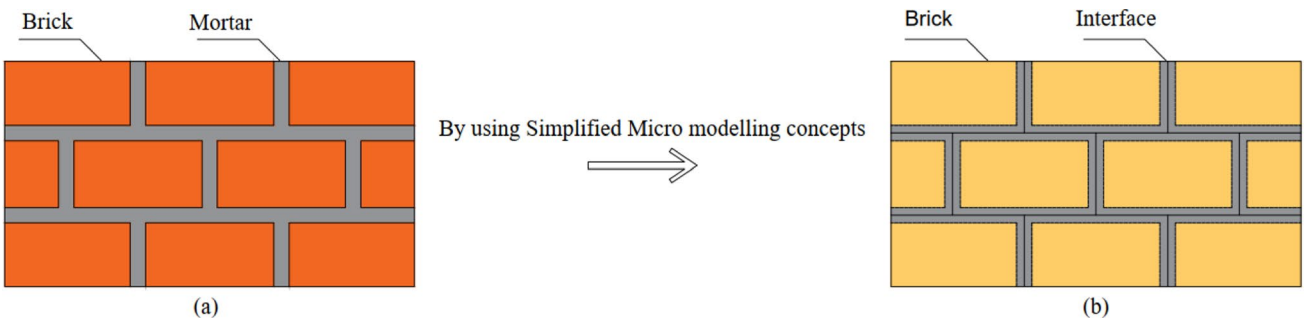

Fig. 5 Different types of micro-modeling (Lourenço 1997) **a** detailed micro-modeling **b** simplified micro-modelling

Table 3 Features of perforated brick interface element (Misir et al. 2018)

Contact properties						
Cohesive behavior (N/mm)			Tangential behavior	Damage		
K_{nn}	K_{ss}	K_{tt}	Coefficient of friction	Normal	Shear-1	Shear-2
70	40	40	0.7	0.23	0.15	0.15

The three-dimensional FEM of the SMW created in ABAQUS is shown in Fig. 6. According to the test setup mentioned in Sect. 2, the connection of the horizontal and vertical bars is modeled as pinned supports. During the application of the cyclic loading, contacts occur between the different elements, and the nonlinearity condition of the structure allows discontinuous and instantaneous change. The Quasi-static displacement controlled cyclic loading history used in the tests is given in Fig. 7. The max. lateral displacement for loading history was taken 20 mm according to drift ratio (DR). The drift ratio was taken as %1.33 (Δ/l). In this way, it is aimed to cause enough damage to the wall that can be repaired. The analytical studies are performed to predict the influence of the lateral cyclic loading that generated a bending effect on the wall. A cyclic force which includes back and forth movement of the hydraulic piston corresponds to the tension–compression loads. This piston gradually increases and decreases the forces from −1000 kN for tension to 1000 kN for compression.

The maximum displacement contour diagram of SMW obtained from FEA of simplified micro-modeling wall under cyclic loadings is shown in Fig. 8. These contours represent the distribution of the peak values reached by the maximum displacements at each point within the section. The displacement values increase along to the middle of the SMW and the maximum displacement is obtained as 9.24 mm. The diagonal cracks in a zigzag form observed on the surface of SMW, are caused by the action of cyclic forces which have also changed its resistance capacities.

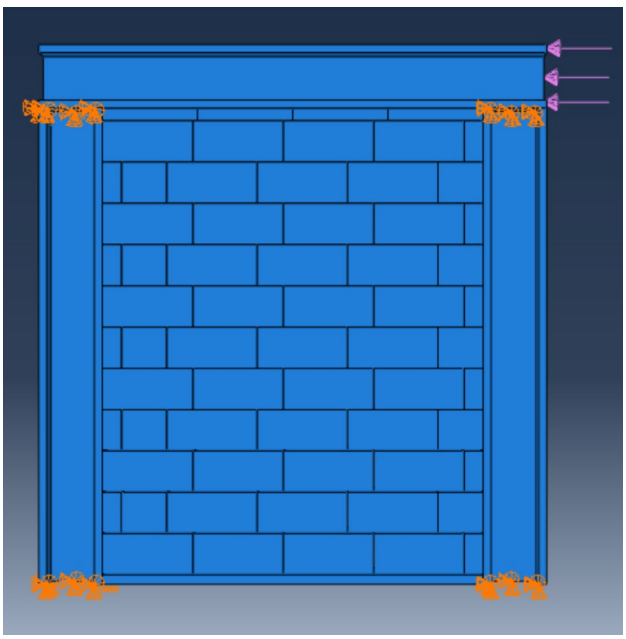

Fig. 6 Boundary conditions and application of lateral cyclic forces

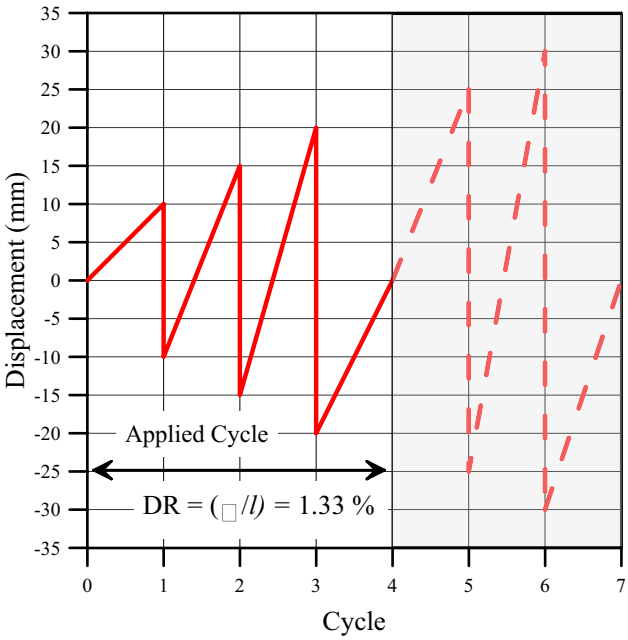

Fig. 7 Protocol of cyclic loadings application

In the experimental tests, the loading protocol shown in Fig. 7 was applied to the elements of the frame sample by the hydraulic piston. The lateral load protocol applied to the elements of the frame sample was given in the form of bidirectional incremental displacement cycles (push and pull). To obtain test data on the masonry frame in a healthy way, cracks in the walls were observed, and the displacement value at the load and at the place of measurement was monitored with many instruments consisting of the LPDT and pressure sensors was registered with the data collection system. There was no special specification for the contacts between the steel and the masonry bricks. The masonry structure was simply built inside the steel frame. However, in the modeling, the orientation of the steel surfaces that acted on the surfaces of the bricks was used as the "master

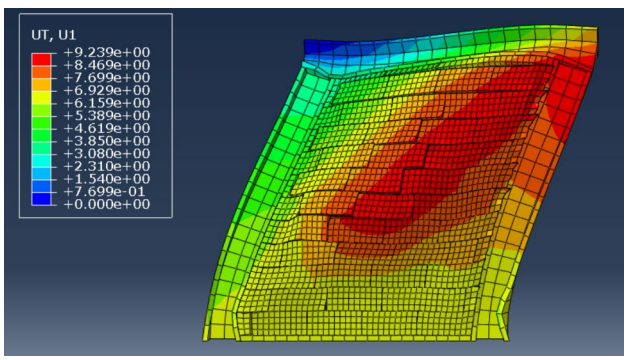

Fig. 8 Analytical results of simplified micro-modeling wall under cyclic loadings

surface" and those which underwent the forces were used as the "slave surface". Moreover, the stiffest body was taken as the master surface and the least stiff as the slave surface as recommended by the ABAQUS software.

After the application of the cyclic loadings on the SMW, it was noticed a long diagonal crack interspersed by two other cracks (Fig. 9). The first crack went in the direction that was obtained from the analytical test of micro-modeling. As for the other two cracks, they seemed to come out, due to the excessive handling of the loads during the experiment.

The hysteresis curve for damaged SMW is given in Fig. 10. This curve gives the variation of the loads and their displacements caused as the force which was applied to the wall increases or decreases. The graph shows that the maximum loads are 99.91 and −103.04 kN. The first peak load is reached when the displacement is about 9.13 mm. This is like the 9.24 mm displacement obtained during the analysis FEM of the micro-modeling of the masonry wall. There was a 2.81% difference between experimental and analytical studies. The load corresponding to a 1% drift ratio is obtained as 66.13 kN.

The damaged SMW was rehabilitated with mortar to implement CFRP easily. CFRPs are composite materials and contain at least two immiscible components with complementary properties. The composite materials consist of a continuous phase (the resin) and reinforcement (carbon). The resin ensures the cohesion of the structure and the transmission of the mechanical forces towards the reinforcement. The wall having been damaged, is reinforced to regain its initial mechanical properties fully or almost. Carbon fibers are less sensitive to creep and fatigue whereas the Epoxy matrix improves the adhesion of FRP to substrates. It maintains the fiber orientation and improves the transfer of stresses from substrates to fibers.

MBrace Fiber CF 230/4900 type carbon fiber reinforced polymer produced by BASF (BASF 2016) was used. Some technical properties are given in Table 4 (Altunişik et al. 2018). Epoxy, which consisted of two components, namely, epoxy resin and epoxy hardener primer (BASF-MBrace Primer) was applied to the wall surfaces. The properties of the MBrace Fiber Saturant adhesive are given in Table 5 (Altunişik et al. 2018). Carbon fibers were cut into sheets 140 cm long and 25 cm wide. These were glued diagonally as some cracks appeared before. Then another cutting of the carbon was performed to rectangular dimensions of 34 cm in length and 25 cm in width. They were placed on the wall at the four sides of a surface as it is presented in Fig. 11.

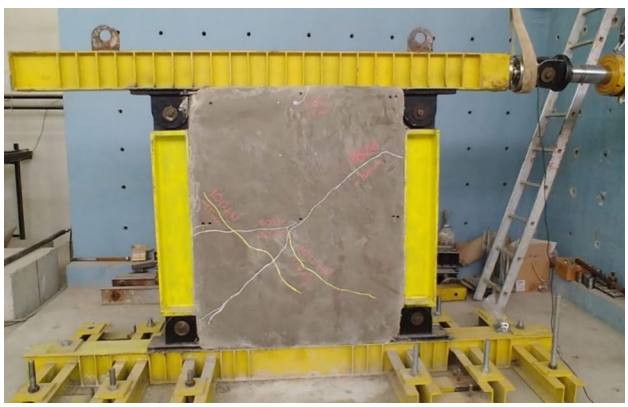

Fig. 9 Experimental damaged SMW

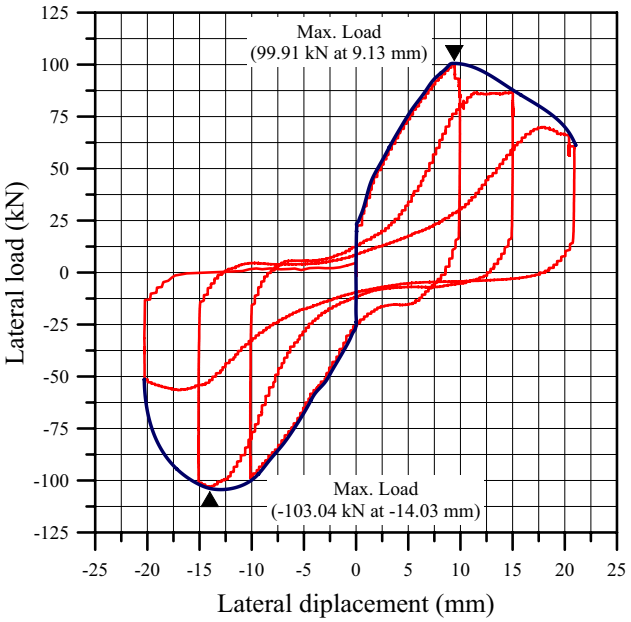

Fig. 10 Hysteresis curve for damaged SMW

The CFRP-coated SMW was exposed to the same load protocol as SMW. The hysteresis curve for coated SMW is given in Fig. 12. The graph shows that the maximum loads are 75.91 and −117.56 kN. The first peak load is reached when the displacement is about 13.83 mm. When the results of the cyclic load test for undamaged and retrofitted SMW were compared, it was clearly seen that it regained its initial mechanical properties fully or almost.

Table 4 The properties of CFRP fabric

Properties	Mbrace fibre CF 230/4900 200 g/m^2
Young's modulus (MPa)	230,000
Tensile strength (MPa)	4900
Design cross-section thickness (mm)	0.111
Total fiber weight (g/m^2)	210
Elongation at break (%)	2.10
Width (mm)	500

Table 5 The properties of Mbrace fiber saturant adhesive

Material	
Mbrace fibre saturant component A	Epoxy resin
Mbrace fibre saturant component B	Epoxy hardener
Color	Blue
Mixture density	1.02 kg/lit
Viscosity	1500–2500 mPa s
Compression strength (7 days)	> 60 MPa
Bending strength (7 days)	> 50 MPa
Adhesive strength (to concrete-7 days)	> 3 MPa
Applicable soil temperature	+ 5 ℃ + 30 ℃
Re-coatability duration (+ 20 ℃)	Minimum 48 h-maximum 7 days
Usage time	30 min
Total cure time	7 days

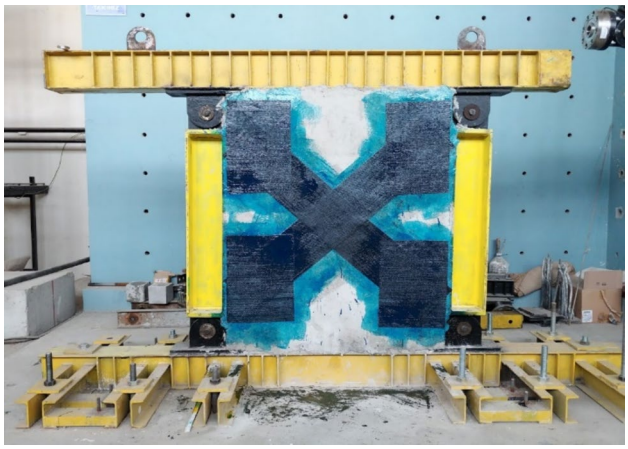

Fig. 11 The damaged SMW coated with CFRP material

Load–displacement envelopes were obtained from peak load and displacement at the end of the first cycle of every loading step. Load–displacement envelopes for all specimens are given in Fig. 13. The damaged SMW achieved a greater peak load at the push direction whereas the CFRP-coated SMW achieved it at the pull direction.

4 Modal Analysis

The modal analysis was performed to determine the natural frequency and shape modes of the masonry wall. In this type of analysis, a new step related to frequency was chosen in the ABAQUS software program. Parameters were redefined since this analysis did not respond to the same principles as the previous analysis (simplified micro-modeling analysis).

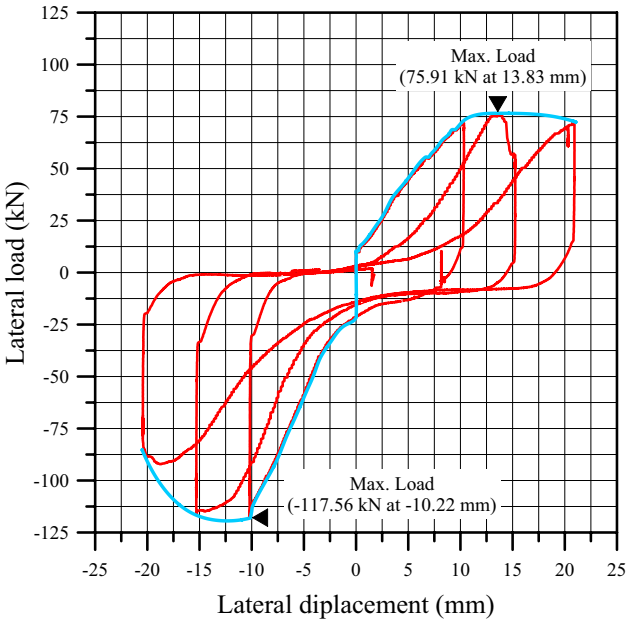

Fig. 12 Hysteresis curve for CFRP-coated damaged wall

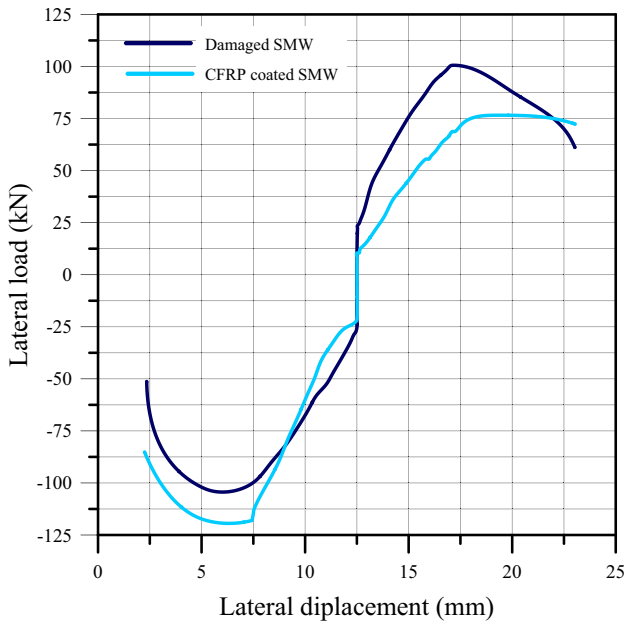

Fig. 13 Load displacement envelopes

Lanczos' iterative procedure was chosen in the software to get modal responses.

The operational modal analysis (OMA) was evaluated in this paper to identify modal parameters. It is also an assessment of the dynamic properties of structures in an experimental way with a view to upgrading their dynamic characteristics. This evaluation is often carried out on historical structures (Alaggio et al. 2021; Lorenzoni et al. 2017; Ceravolo et al. 2016) after

an earthquake, and or earthquake simulation by shaking table or, the cyclic loading (Ghezelbash et al. 2020; Qin et al. 2021; Mojsilović and Salmanpour 2016). Many modal parameter identification techniques have been developed by researchers for different uses. In this study, the enhanced frequency domain decomposition (EFDD) method in the frequency domain, and the more advanced stochastic subspace identification (SSI) method in the time domain among these techniques were implemented to extract the modal parameters.

4.1 Enhanced Frequency Domain Decomposition (EFDD) Method

The EFDD method is primarily since the frequency response function goes through an extreme around the natural frequencies. In the context of ambient vibration measurements, the frequency response function is replaced by the auto spectra of the output-only data. To include the measurement channels of all setups, the average normalized power spectral densities (ANPSDs) are used. In such a way, the identified natural frequencies are simply obtained from the observation of the peaks on the graphs of ANPSDs.

The relationship between the input x(t) and the output y(t) can be written (Bendat and Piersol (1986); (Felber (1993)):

$$\left[G_{\mathbf{yy}}(\omega)\right] = [H(\omega)]^{*}\left[G_{\mathbf{xx}}(\omega)\right][H(\omega)]^{T} \tag{3}$$

where $G_{\mathbf{xx}}$ is the Power Spectral Density (PSD) matrix of the input, $G_{\mathbf{yy}}$ is the PSD matrix of the output, H is the Frequency Response Function (FRF) matrix, and * and T denote complex conjugate and transpose respectively. After some mathematical manipulations the output PSD can be reduced to a pole/residue form as follows Bendat and Piersol (1986):

$$\left[G_{yy}(\omega)\right] = \sum_{k=1}^{m}\left(\frac{[A_k]}{j\omega-\lambda_k} + \frac{[A_k]^{*}}{j\omega-\lambda_k^{*}} + \frac{[B_k]}{-j\omega-\lambda_k} + \frac{[B_k]^{*}}{-j\omega-\lambda_k^{*}}\right) \tag{4}$$

where A_k is the *k-th* residue matrix of the output PSD. The response spectral density matrix can be written in the following final form considering a lightly damped system Bendat and Piersol (1986):

$$\left[G_{yy}(\omega)\right] = \sum_{k=Sub(\omega)}\left(\frac{d_k\psi_k\psi_k^{T}}{j\omega-\lambda_k} + \frac{d_k^{*}\psi_k^{*}\psi_k^{T}}{j\omega-\lambda_k^{*}}\right) \tag{5}$$

where d_k is a scalar constant and ψ_k is the k-th mode shape vector. Thus, performing the singular value decomposition of the output PSD matrix known at discrete frequencies $\omega-\omega_i$ one obtains Bendat and Piersol (1986):

$$\hat{G}_{yy}(j\omega_i) = U_iS_iU_i^{H} \tag{6}$$

where the matrix U_i is a unitary matrix holding the singular vector u_{ij} and S_i is a diagonal matrix holding the scalar singular values s_{ij}; the superscript H denotes complex conjugate and transpose. Near a peak corresponding to the *k-th* mode in the spectrum, only the *k-th* mode is dominant, and the PSD matrix approximates to a rank one matrix as Bendat and Piersol (1986):

$$\hat{G}_{yy}(j\omega_i) = s_iu_{i1}u_{i1}^{H},\ \omega_i \to \omega_k \tag{7}$$

The first singular vector at the r-th resonance is an estimate of the *r-th* mode shape Bendat and Piersol (1986):

$$\hat{\phi}_r = u_{r1} \tag{8}$$

4.2 Stochastic Subspace Identification (SSI) Method

The stochastic subspace identification technique is a time-domain method that directly works with time data, without the need to convert them to correlations or spectra. The stochastic subspace identification algorithm identifies the state space matrices based on the measurements by using robust numerical techniques. Once the mathematical description of the structure (the state space model) is found, it is straightforward to determine the modal parameters. The theoretical background is given in by Overschee and Moor (1996), as well as Peeters (Software 2006). The model of vibration structures can be defined by a set of linear, constant coefficient and second-order differential equations (Peeters 2000):

$$M\ddot{U}(t) + C_{*}\dot{U}(t) + KU(t) = F(t) = B_{*}u(t) \tag{9}$$

where M, C_{*}, K are the mass, damping and stiffness matrices, $F(t)$ is the excitation force, and $U(t)$ is the displacement vector at continuous time t. Observe that the force vector $F(t)$ is factorized into a matrix B_{*} describing the inputs in space and a vector $u(t)$. Although Eqs. (11) represents quite closely the true behavior of a vibrating structure, it is not directly used in SSI methods. So, the equation of dynamic equilibrium (9) will be converted to a more suitable form: the discrete-time stochastic state-space model (Qin et al. 2021). The state-space model originates from control theory, but it also appears in mechanical/civil engineering to compute the modal parameters of a dynamic structure with a general viscous damping model Ewins (1984). With the following definitions,

$$x(t) = \begin{pmatrix} U(t) \\ \dot{U}(t) \end{pmatrix},\ A_c = \begin{pmatrix} 0 & I_{n_2} \\ -M^{-1}K & -M^{-1}C_{*} \end{pmatrix},\ B_c = \begin{pmatrix} 0 \\ M^{-1}B_{*} \end{pmatrix} \tag{10}$$

Equations (12) can be transformed into the state equation

$$\dot{x}(t) = A_cx(t) + B_cu(t) \tag{11}$$

where A_c is the state matrix, B_c is the input matrix and $x(t)$ is the state vector. The number of elements of the state-space vector is the number of independent variables needed to describe the state of a system. If it is assumed that the measurements are evaluated at only one sensor locations, and that these sensors can be accelerometers, velocity or displacement transducers, the observation equation is Peeters (2000):

$$y(t) = C_a\ddot{U}(t) + C_v\dot{U}(t) + C_dU(t) \tag{12}$$

where $y(t)$ are the outputs, and C_a, C_v, C_d, are the output matrices for displacement, velocity, acceleration. With the following definitions (Peeters (Software 2006)),

$$\left.\begin{aligned} C &= \left[\, C_d - C_aM^{-1}K \;\; C_v - C_aM^{-1}C_* \,\right] \\ D &= C_aM^{-1}B_* \end{aligned}\right\} \tag{13}$$

Equations (12) can be transformed into:

$$y(t) = Cx(t) + Du(t) \tag{14}$$

where C is the output matrix and D is the direct transmission matrix. Equations (11) and (14) constitute a continuous-time deterministic state-space model. Continuous time means that the expressions can be evaluated at each time instant $t\in \mathbb{R}$ and deterministic means that the input–output quantities $u(t)$, $y(t)$ can be measured exactly. Of course, this is not realistic: measurements are available at discrete time instants $k\Delta t$, $k \in \mathbb{N}$ with Δt, the sample time and noise is always influencing the data. After sampling, the state-space model looks like:

$$\left.\begin{aligned} x_{k+1} &= Ax_k + Bu_k \\ y_k &= Cx_k + Du_k \end{aligned}\right\} \tag{15}$$

where $x_k = x(k\Delta t)$ is the discrete-time state vector, $A = \exp(A_c\Delta t)$ is the discrete state matrix and $B = [A - I]A_c^{-1}B_c$ is the discrete input matrix. If A_c is not invertible, another expression holds for B. The stochastic components (noise) are included, and we obtain the following discrete-time combined deterministic-stochastic state-space model:

$$\left.\begin{aligned} x_{k+1} &= Ax_k + Bu_k + w_k \\ y_k &= Cx_k + Du_k + v_k \end{aligned}\right\} \tag{16}$$

where w_k is the process noise due to disturbances and modeling inaccuracies and v_k is the measurement noise due to sensor inaccuracy. They are both immeasurable vector signals, but we assume that they are zero mean, white and with covariance matrices Peeters (2000):

$$E\left[\begin{pmatrix} w_p \\ v_p \end{pmatrix}\begin{pmatrix} w_q^T & v_q^T \end{pmatrix}\right] = \begin{pmatrix} Q & S \\ S^T & R \end{pmatrix}\delta_{pq} \tag{17}$$

where E is the expected value operator and δ_{pq} is the Kronecker delta.

The vibration information that is available in structural health monitoring is usually the responses of a structure excited by the operational inputs that are some immeasurable inputs. Due to the lack of input information, it is impossible to distinguish deterministic input u_k from the noise terms w_k, v_k in Eqs. (16). If the deterministic input term u_k is modeled by the noise terms w_k, v_k the discrete-time purely stochastic state-space model of a vibration structure is obtained:

$$\left.\begin{aligned} x_{k+1} &= Ax_k + w_k \\ y_k &= Cx_k + v_k \end{aligned}\right\} \lim_{x\to\infty} \tag{18}$$

Equations (18) constitutes the basis for the time-domain system identification through operational vibration measurements. The SSI method identifies the state-space matrices based on the output only measurements and by using robust numerical techniques.

OMA was performed to identify the exact dynamic characteristic of structures with the help of response vibrations. These response vibrations were acquired from structures, recorded at the data bank, and then sent for the processing phase with the help of Labshop (2006) and Software (2006) which were operated through EFDD and SSI techniques. The uni-axial seismic accelerometers (BK4507) were used to measure the response signal. To measure the exact structural response, enough points were determined on the front surface of the SMW and totally eight accelerometers were mounted. The location of the mounted point of accelerometers on SMW is shown in Fig. 14. The measurements were continued 20 min and

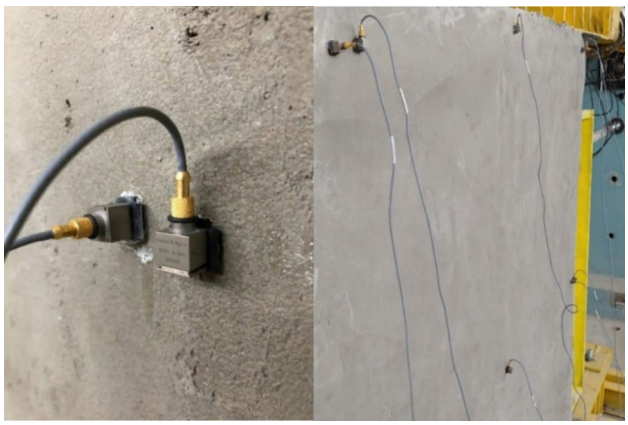

Fig. 14 The location of the mounted point of accelerometers on SMW

a hammer was used to vibrate the SMW to provide that all modes of the SMW were obtained easily. Response signals that occurred from the vibrations were measured by accelerometers then these signals were recorded with a data system and sent to a computer equipped with OMA software. This software was analyzed the collected signal with the help of EFDD and SSI techniques. At the end of the analysis exact dynamic characteristics such as, mode shapes and natural frequencies of SMW were obtained. The experimental data were collected and compared with those obtained through the analytical method for undamaged, damaged and CFRP-coated SMW separately in later sections.

5 The results of the Modal Analysis

5.1 Analytical and Experimental Modal Analysis Results for Undamaged SMW

The comparison of mode shapes and natural frequencies of the SMW obtained from analytically and experimentally are given in Fig. 15 and Table 6, respectively. By carefully observing mode 1, it is noted that the movement of the modal tension was carried out in the XZ plane. So, the top of the wall was a uniform movement starting from the X coordinates towards Z (i.e. the wall tends to lean towards Z). Mode 2 performs a kind of torsion on itself in the XY plane. The movement takes place by pulling the sides out and trying to rotate on its own. The mode shapes of the wall

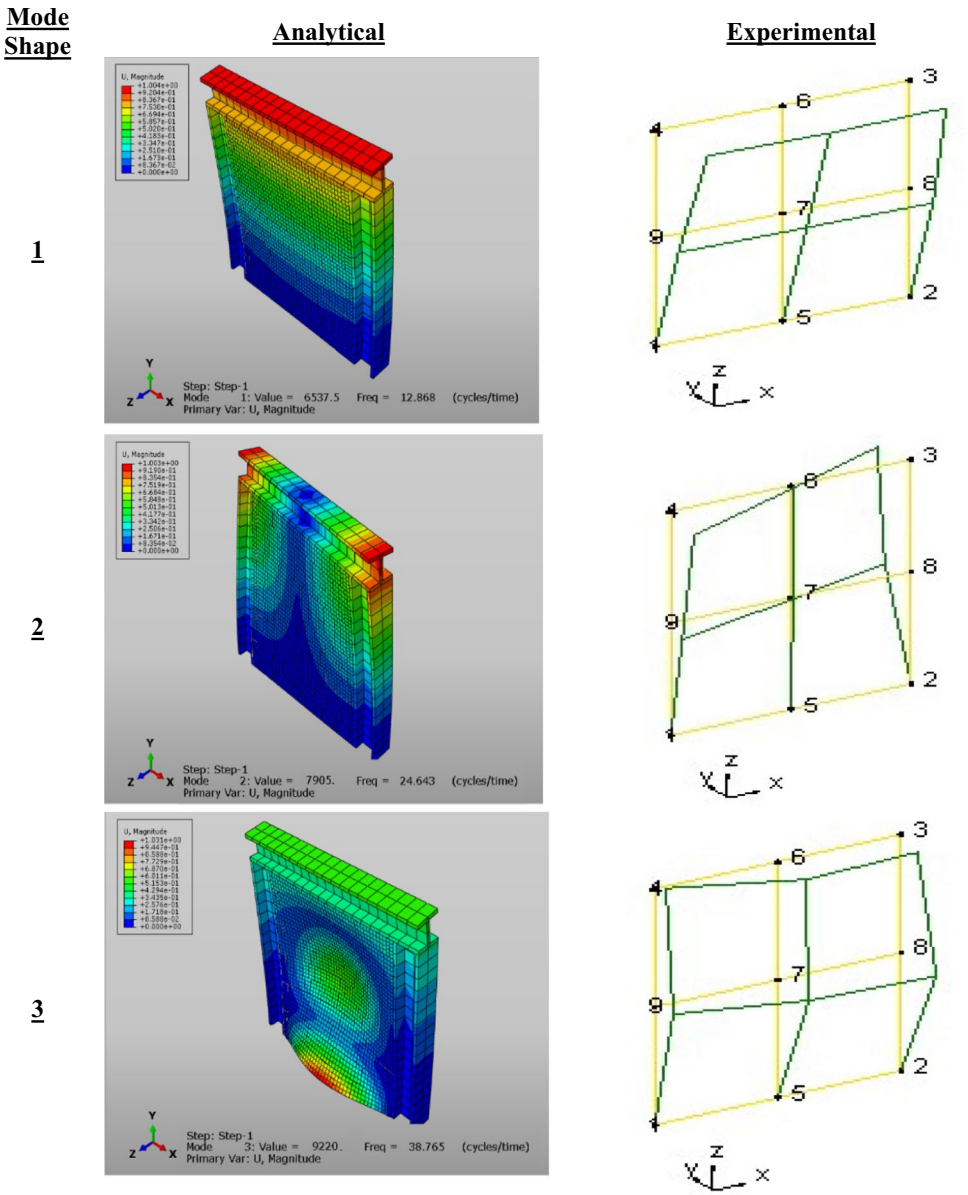

Fig. 15 The comparison of mode shapes

Table 6 The comparison of natural frequencies of undamaged SMW

Mode shape	Analytical frenquency (Hz)	Experimental frequency (Hz)	Percentage of error (%)
1	12.87	12.62	1.94
2	24.64	25.02	1.54
3	38.76	38.36	1.031

start to move from right to left. Mode 3 performs a concave movement mainly towards the center of the wall. It is clearly seen from Fig. 15 that the mode shapes of SMW obtained from FEM modal analysis and OMA overlap. The differences between the values of natural frequencies determined from FEM modal analysis and OMA are fewer than %2.

5.2 Experimental Modal Analysis Results for Damaged SMW

After the application of the cyclic loadings, the damaged SMW (Fig. 16) was evaluated to determine its frequencies and its mode shapes only experimentally. The mode shapes and natural frequencies of first three modes of SMW obtained from OMA are given in Fig. 17. The comparison of the results of the damaged SMW with those of the undamaged SMW shown, mode shapes which are similar to each

Fig. 16 Operational modal analysis on damaged SMW

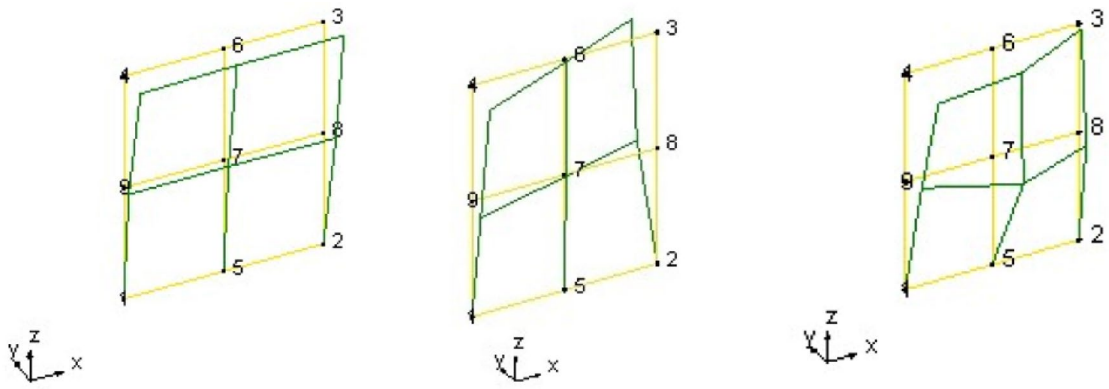

Fig. 17 Mode shapes and frequencies for experimental SMW damaged. **a** Mod 1 (9.84 Hz), **b** Mod 2 (21.64 Hz), **c** Mod 3 (36.25 Hz)

other. It is clearly seen that decreasing of natural frequencies due to the decrease in stiffness, which is implicitly linked to the formula of the frequency.

5.3 Experimental Modal Analysis Results for Retrofitted with CFRP SMW

After retrofitting the damaged SMW with CFRP, OMA was applied to determine its frequencies and its mode shapes (Fig. 18). The mode shapes and natural frequencies of the first three modes of SMW retrofitted with CFRP obtained from OMA are given in Fig. 19. By comparing the results of the damaged SMW with those of the retrofitted SMW, mode shapes, and frequencies are changed. It was seen that an increase in natural frequencies due to the increase in stiffness was implicitly linked to the formula of the frequency. Furthermore, natural frequencies of retrofitted SMW were higher than undamaged SMW.

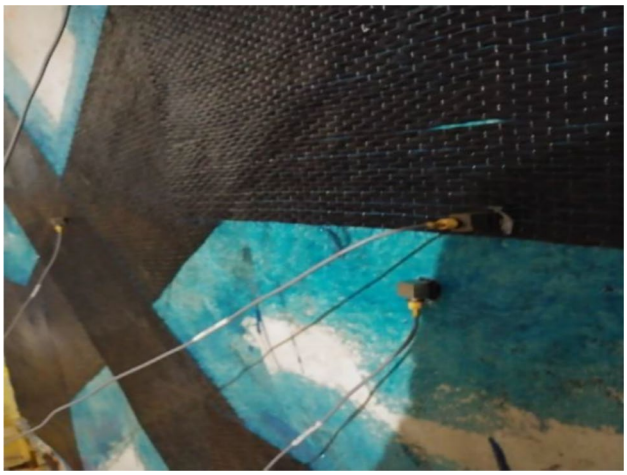

Fig. 18 Operational modal analysis on damaged SMW

6 Conclusion

This paper aims to present the results of experimental and analytical investigations of unreinforced masonry walls (URM) exposed to continuous tensile-compressive cyclic loading and operational modal analysis. For the experimental investigation, a sample masonry wall (SMW) was designed inside a rectangular steel frame carried by pinned supports and built over 1200 mm in length by 1500 mm in height. After the influence of cyclic loading damaged SMW was retrofitted by CFRP. The retrofitted SMW underwent the same cyclic loading to obtain the effects of CFRP on the load–displacement capacity of the damaged masonry wall. Furthermore, an operational modal analysis test was conducted over SMW (undamaged, damaged, and retrofitted with CFRP) to determine their real dynamic characteristics. For analytical investigations, finite element analysis (FEA) was implemented in ABAQUS software with a simplified micro-modeling approach, and damages were considered only in terms of displacement in this work. Nonlinear cyclic analysis was performed to obtain crack patterns and displacements. To determine modal parameters such as mode shapes and frequencies, modal analysis was also conducted. The obtained results such as displacements, damage patterns, and modal parameters from analytical investigations were compared with experimental investigations. These different stages of these investigations provided globally satisfactory results:

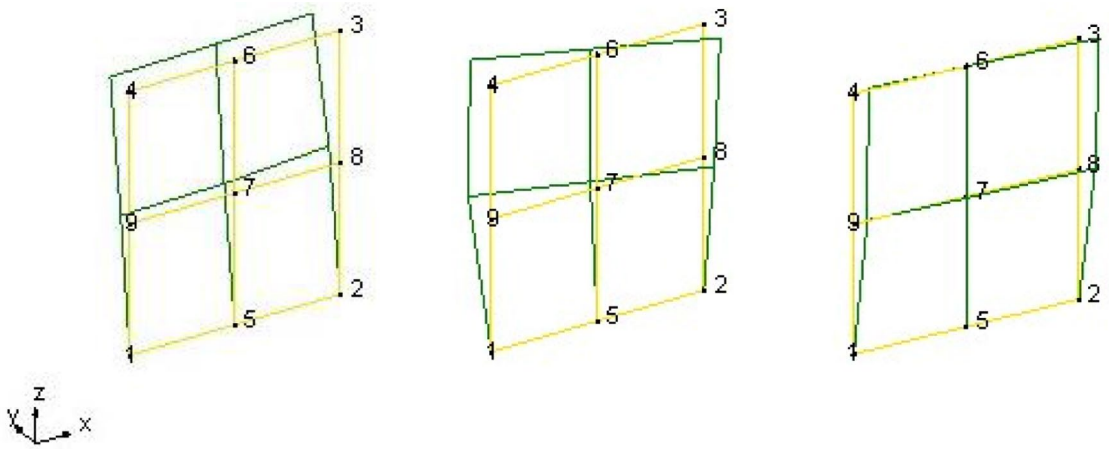

Fig. 19 Mode shapes and frequencies for experimental SMW-damaged. **a** Mod 1 (15.37 Hz), **b** Mod 2 (29.51 Hz), **c** Mod 3 (41.78 Hz)

- The result of FEA shows that the displacement values increase along the middle of the SMW. The diagonal cracks in a zigzag form observed on the surface of SMW, were caused by the action of cyclic forces which have at the same time changed their resistance capacities.
- After the experimental application of the cyclic loadings on the SMW, it is noticed a long diagonal crack interspersed by two other cracks. The first crack goes in the direction obtained from the analytical test of micro-modeling. As for the other two cracks, they seem to come out, due to the excessive handling of the loads during the experiment.
- The FEA and experimental test results show that the difference between the result of the FEA and experimental test is 2.81%.
- The damaged SMW is retrofitted by CFRP and then underwent the same cyclic loading. When the results of the cyclic load test for undamaged and retrofitted SMW are compared it is clearly seen that it regains its initial mechanical properties fully or almost.
- In comparison between the analytical and operational modal analysis results for undamaged SMW, the mode shapes are similar, and frequencies are close to each other. Error percentages in frequencies are less than 2%.
- When the dynamic characteristics of the damaged SMW and undamaged SMW are compared, it is seen that the mode shapes of two SMW are the same, but the frequencies of damaged SMW have decreased. The decrease is between 22 and 25%
- As for strengthening the damaged SMW with CFRP it has been seen that mode shapes and natural frequencies are changed. Using CRFP for the retrofitting of damaged SMW increases the frequencies from 26 to 36%. There is an increase from 15 to 17.89% in frequency when comparing the CFRP wall with the undamaged wall. This indicates that FRP helps restore resistance properties. Since the mass is the same, it is the stiffness of the wall that gains resistance with CFRP.

Acknowledgements The authors would like to acknowledge Prof. Dr. Metin Hüsem, Prof. Dr. Süleyman Adanur, Prof. Dr. Ahmet Can Altunışik, Assoc. Prof. Murat Günaydın and Assoc. Prof. Serhat Demir for their support in conducting the experiments.

Funding This work was supported by the Scientific Research Projects Coordination Unit of Karadeniz Technical University. The project number is FBA-2019-8074.

Declarations

Conflict of interest The authors declare that they have no conflict of interest.

References

ABAQUS online documentation (2014) Simulia Inc.

Abdulla KF, Cunningham LS, Gillie M (2017) Simulating masonry wall behaviour using a simplified micro-model approach. Eng Struct 151:349–365. https://doi.org/10.1016/j.engstruct.2017.08.021

Alaggio R, Aloisio A, Antonacci E, Cirella R (2021) Two-years static and dynamic monitoring of the Santa Maria di Collemaggio basilica. Constr Build Mater 268:121069

Ali HT, Akrami R, Fotouhi S, Bodaghi M, Saeedifar M, Yusuf M, Fotouhi M (2021) Fiber reinforced polymer composites in bridge industry. Structures 30:774–785. https://doi.org/10.1016/j.istruc.2020.12.092

Altunişik AC, Karahasan OŞ, Genç AF, Okur FY, Günaydin M, Kalkan E, Adanur S (2018) Modal parameter identification of RC frame under undamaged, damaged, repaired and strengthened conditions. Measurement 124:260–276

Aref AJ, Dolatshahi KM (2013) A three-dimensional cyclic meso-scale numerical procedure for simulation of unreinforced masonry structures. Comput Struct 120:9–23

BASF (2016) The chemical company. Ludwigshafen, Germany

Bendat JS, Piersol AG (1986) Random data: analysis and measurement procedures. John Wiley & Sons, USA

Bernat-Masó E, Gil L (2019) Assessing the performance of CFRP strengthening on masonry walls using modal analysis. Eng Struct 193(2):184–193. https://doi.org/10.1016/j.engstruct.2019.05.036

Bolhassani M, Hamid AA, Lau ACW, Moon F (2015) Simplified of micro modeling of partially grouted masonry assemblages. Constr Build Mater 83:159–173. https://doi.org/10.1016/j.conbuildmat.2015.03.021

Ceravolo R, Pistone G, Fragonara LZ, Massetto S, Abbiati G (2016) Vibration-based monitoring and diagnosis of cultural heritage: a methodological discussion in three examples. Int J Archit Herit 10(4):375–395. https://doi.org/10.1080/15583058.2013.850554

Chaimoon K, Attard MM (2007) Modeling of unreinforced masonry walls under shear and compression. Eng Struct 29(9):2056–2068. https://doi.org/10.1016/j.engstruct.2006.10.019

TS EN 771-1 (2011) Properties of masonry units part 1: clay masonry units (bricks). Turkish Standards Institute, Ankara

Ewins DJ (1984) Modal testing: theory and practice. Research Studies Press Ltd, Baldock, Hertfordshire, England

Felber AJ (1993) Development of hybrid bridge evaluation system. PhD Thesis, University of British 447 Columbia, Vancouver, Canada.

Ferris MC, Tin-Loi F (2001) Limit analysis of frictional block assemblies as mathematical program with complementary constrains. Int J Numer Mech Sci 43(1):209–224. https://doi.org/10.1016/S0020-7403(99)00111-3

Ghezelbash A, Beyer K, Dolatshahi KM, Yekrangnia M (2020) Shake table test of a masonry building retrofitted with shotcrete. Eng Struct 219:110912. https://doi.org/10.1016/j.engstruct.2020.110912

Greco F, Leonetti L, Luciano R, Pascuzzo A, Ronchei C (2020) A detailed micro-model for brick masonry structures based on a diffuse cohesive-frictional interface fracture approach. Procedia Struct Integr 25:334–347. https://doi.org/10.1016/j.prostr.2020.04.038

Hamzeh L, Hassanein A, Galal K (2020) Numerical study on the seismic response of GFRP and steel reinforced masonry shear walls with boundary elements. Structures 28:1946–1964

Khatieb ME (2016) Experimental evaluation of concrete fracture energy and its dependency on relevant parameters. Int J Appl Eng Res 20:10348–10352

PULSE. Labshop (2006) Version 11.2.2, Bruel and Kjaer, Sound and vibration measurement A/S, Denmark

Lorenzoni F, Valluzzi MR, Salvalaggio M, Minello A, Modena C (2017) Operational modal analysis for the characterization of ancient water towers in Pompeii. Proced Eng 199:3374–3379

Lotfi HR, Shing PB (1994) Interface model applied to fracture of masonry structures. J Struct Eng 120(1):63–80. https://doi.org/10.1061/(ASCE)0733-9445(1994)120:1(63)

Lourenço PB (1997) Computational strategies for masonry structures. PhD Thesis. Delft University of Technology.

Lourenço PB, Rots JG (1997) Multisurface interface model for analysis of masonry structures. J Eng Mech 123(7):660–668. https://doi.org/10.1061/(ASCE)0733-9399(1997)123:7(660)

Malomo D, Dejong MJ (2021) A macro-distinct element model (M-DEM) for out-of-plane analysis of unreinforced masonry structures. Eng Struct 244:112754. https://doi.org/10.1016/j.engstruct.2021.112754

Marcari G, Manfredi G, Prota A, Pecce M (2007) In-plane shear performance of masonry panels strengthened with FRP. Compos Part B Eng 38:887–901. https://doi.org/10.1016/j.compositesb.2006.11.004

Milani G, Taliercio A (2016) Limit analysis of transversally loaded masonry walls using an innovative macroscopic strength criterion. Int J Solids Struct 81:274–293

Misir IS, Youssouf IB, Yucel G (2018) Out-of-plane damage limits for the walls in historical URM Buildings under earthquake actions: a case Study for Isabey Mosque. In: 3th International conference on civil and environmental engineering Cesme, Izmir, Turkey

Mojsilović N, Salmanpour AH (2016) Masonry walls subjected to in-plane cyclic loading: application of digital image correlation for deformation field measurement. Int J Mason Res 1(2):165–187

Oliveira DV, Lourenço PB (2004) Implementation and validation of a constitutive model for the cyclic behaviour of interface elements. Comput Struct 82(17):1451–1461

Oschsendorf J, De Lorenzis L (2001) Failure of rectangular masonry buttresses under concentrated loading. Proceedings of the institution of civil engineers—structures and buildings, 161:265-75. https://doi.org/10.1680/stbu.2008.161.5.265.

Page AW (1978) Finite element model for masonry. J Struct Div 104(8):1267–1285

Peeters B (2000) System Identification and Damage Detection in Civil Engineering. PhD Thesis, K.U, Leuven, Belgium.

Pulatsu B, Gonen S, Erdogmus E, Lourenço PB, Lemos JV, Prakash R (2021) In-plane structural performance of dry-joint stone masonry Walls: A spatial and non-spatial stochastic discontinuum analysis. Eng Struct 242:112620. https://doi.org/10.1016/j.engstruct.2021.112620

Qin C, Bai G, Wu T, Wang B, Fu G (2021) Seismic behavior of unreinforced and confined masonry walls using innovative sintered insulation shale blocks under cyclic in-plane loading. Constr Build Mater 268:121063. https://doi.org/10.1016/j.conbuildmat.2020.121063

Restuccia L, Ferro GA, Suarez-Riera D, Sirico A, Bernardi P, Belletti B, Malcevschi A (2020) Mechanical characterization of different biochar-based cement composites. Proced Struct Integr 25:226–233. https://doi.org/10.1016/j.prostr.2020.04.027

Russell J, Wei X, Živanović S, Kruger C (2017) Dynamic response of an FRP footbridge due to pedestrians and train buffeting. Procedia Eng 199:3059–3064. https://doi.org/10.1016/j.proeng.2017.09.411

Santa-Maria H, Alcaino P (2011) Repair of in-plane shear damaged masonry wall with external FRP. Constr Build Mater 25:1172–1180. https://doi.org/10.1016/j.conbuildmat.2010.09.030

Sarhosis V, Lemos JV (2018) A detailed micro-modelling approach for the structural analysis of masonry assemblages. Comput Struct 206:66–81. https://doi.org/10.1016/j.compstruc.2018.06.003

Sesli H, Husem M (2021) Experimental investigation on cyclic behavior of reinforced concrete coupling beams under quasi-static loading. Int J Civil Eng 19(4):381–400

Smits J (2016) Fiber-reinforced polymer bridge design in the Netherlands: architectural challenges toward innovative, sustainable, and durable bridges. Engineering 2(4):518–527

OMA Software (2006) Operational modal analysis. Release 4.0, Structural Vibration Solution A/S, Denmark

Stratford T, Pascale G, Manfroni O, Bonfiglioli B (2004) Shear strengthening masonry panels with sheet glass-fiber reinforced polymer. J Compos Constr 8(5):434–443

Uyttersprot J, De Corte W, Ingelbinck B (2021) Influence of SLS design requirements on the material consumption and self-weight of web-core sandwich panel FRP composite footbridges. Compos Struct 262:113334. https://doi.org/10.1016/j.compstruct.2020.113334

Van Overschee P, De Moor B (1996) Subspace identification for linear systems: theory-488 implementation-applications. Kluwer Academic Publishers, Dordrecht, Netherlands